

Influence of the Pyrolytic Temperature and Feedstock on the Characteristics and Naphthalene Adsorption of Crop Straw-derived Biochars

Enzhu Hu,^{a,*} Siyao Shang,^a Nana Wang,^a Xiangli Nan,^a Shengjun Zhong,^a and Zaijian Yuan^b

The feedstock type and pyrolytic temperature used in producing biochar influence the characteristics of the obtained product and affect the adsorption behavior of naphthalene. In this study, different biochars were pyrolyzed from wheat straw, soybean straw, and corn straw at four temperatures (400 °C to 700 °C). Analyses of the elemental composition, pH, ash content, and specific surface area, scanning electron microscopy, and Fourier transform infrared spectroscopy were performed. The adsorption variations of the naphthalene for the different biochars were evaluated. The results showed that as the pyrolytic temperature increased, the carbon content, ash content, and pH of the biochars increased, the hydrophilicity, aromaticity, and polarity decreased, and the naphthalene adsorption was enhanced. The pseudo-second-order model fit the naphthalene adsorption kinetics better. Both the Langmuir and Freundlich isotherm models confirmed that naphthalene adsorption by all of the produced biochars were effective. Under moderate pyrolytic temperatures, the soybean straw-derived biochar showed a greater naphthalene adsorption capacity and faster adsorption rate than the wheat straw- and corn straw-derived biochars. This study provides a theoretical basis for selecting crop residues and optimizing the pyrolytic temperature with a high efficiency of naphthalene removal from water.

Keywords: Biochar; Crop residue; Pyrolytic temperature; Naphthalene; Adsorption kinetics; Adsorption isotherm

Contact information: a: Institute of Resources and Environmental Sciences, School of Metallurgy, Northeastern University, Shenyang, Liaoning 110819, China; b: Guangdong Key Laboratory of Agro-environmental Pollution Control and Management, Guangdong Institute of Eco-environmental Science & Technology, Guangzhou, Guangdong 510650, China; *Corresponding author: huez@smm.neu.edu.cn

INTRODUCTION

Biochar is a carbon-rich substance with a porous structure derived from pyrolyzed biomass under oxygen-limited conditions at relatively low temperatures (usually 200 to 900 °C) (Ahmad *et al.* 2014; Cha *et al.* 2016). It is presently receiving great attention for being a climate-friendly soil fertilizer and effective sorbent (Wang *et al.* 2018). Because of its particular physical and chemical properties, such as a high specific surface area (S_{BET}), high density of negative surface charges, and characteristic pores and surface functional groups, biochar has shown a favorable adsorption capacity for heavy metals and organic compounds (Pan *et al.* 2013; Xi and Chen 2014).

Naphthalene is a nonpolar hydrophobic organic contaminant and common polycyclic aromatic hydrocarbon. It is the coking co-product of coal tar and petroleum distillation, and it is widely distributed in the environment (Yang *et al.* 2017). Naphthalene in natural water mainly comes from urban domestic sewage, industrial wastewater, atmospheric deposition, and soil leaching (Xi and Chen 2014). Its removal has been widely studied (Cooper *et al.* 2002; Goel *et al.* 2003; Ali and Tarek 2012). However, some typical treatment methods, such as chlorination, oxidation, and ultrasonic irradiation, are not effective because of the low solubility and resistance to mineralization of naphthalene (Changchaivong and Khaodhiar 2009). The adsorption method has been considered one of the most promising techniques because it has a high efficiency and economic performance (Bayazit *et al.* 2017). Among currently developed sorbents, biochars are distinctly advantageous because of the lower cost and abundant sources of biomass.

The properties and adsorption capacities of biochars are primarily ascribed to the nature of the feedstock (Conz *et al.* 2017; Zhang *et al.* 2017; Han *et al.* 2018; Mandal *et al.* 2018; Rodríguez-Vila *et al.* 2018). Moreover, the element composition, surface area, pore volume, and adsorptive characteristics of biochars are different when they are produced at different pyrolytic temperatures (Chen *et al.* 2014; Gai *et al.* 2014; Zhang *et al.* 2015; Tran *et al.* 2016; Li *et al.* 2017). Even though lessons about naphthalene adsorption can be learned from previous work (e.g., orange peels biochar and pine wood biochar) (Chen and Chen 2009; Chen *et al.* 2012), it is not always possible to extrapolate the specific adsorption characteristics from findings using other biochars, considering their differences in elemental compositions, pore structures, and surface properties.

Agricultural residues, such as wheat straw, soybean straw, and corn straw, are the most common low-cost biomass resources in Northeast China. Traditionally, they are combusted for kitchen fire and home-heating or burned in the field, which results in serious local air contamination. In recent years, the management of crop residues has become a notable issue because of the enormous quantities generated and associated environmental constraints (Zhang and Cao 2015; Chen *et al.* 2017; Mehmood *et al.* 2018). Also, these crop residues are generally considered to be favorable feedstock materials for making biochars because of their environmental and economic viability (Yuan *et al.* 2011; Yang *et al.* 2018). However, the surface characteristics and adsorption behaviors of different straw-derived biochars need to be further explored because of uncertainty.

In this study, biochars derived from three crop residues, *i.e.* wheat straw, soybean straw, and corn straw, at different temperatures (400 °C to 700 °C) were systematically characterized by elemental, pH, ash content, and Brunauer-Emmett-Teller (BET) surface area analyses, scanning electron microscopy (SEM), and Fourier transform infrared (FTIR) spectroscopy to better understand their adsorption mechanisms for naphthalene. Batch adsorption experiments were conducted to establish the naphthalene adsorption kinetics and isotherms, which were used to fit the pseudo-first-order and pseudo-second-order kinetic models, and the Langmuir and Freundlich models. The main objective of this study was to examine the impact of the feedstock material and pyrolytic temperature on the biochar properties and naphthalene adsorption characteristics. And the correlation analyses between the adsorption capability, affinity and rates, as well as the characteristics of the biochars may fulfill the knowledge of adsorption mechanisms.

EXPERIMENTAL

Preparation of the Biochars

Biochar samples were produced with three common crop residues: wheat straw (W-BC), soybean straw (S-BC), and corn straw (C-BC). The raw straw materials were collected from the suburb of Shenyang, China, and they were washed several times with distilled water to remove any impurities. After being oven-dried (70 °C) for 3 d, the straw materials were crushed, ground, and sieved to pass through a 2-mm mesh. Then, they were converted to biochars using a muffle furnace equipped with a N₂ purge to ensure oxygen-limited conditions. The pyrolytic temperature was increased to the desired values of 400 °C, 500 °C, 600 °C, and 700 °C, which was held for 3 h before cooling down to ambient temperature.

Characterization of the Biochars

The elemental contents (C, H, O, and N) of the biochars were determined using an elemental analyzer (Elementer Vario MACRO CUBE, Hanau, Germany). The ash content of the biochars was measured as the mass residual percentage after incinerating the samples in an open crucible in a muffle furnace at 750 °C for 4 h, which was modified from a American Society for Testing and Materials (ASTM) standard method (D 1762-84) (ASTM 2007). The weight of the samples was measured after cooling them to room temperature in a desiccator. The pH of the biochars was measured with a digital pH meter (PHS-3C, Leici, Shanghai, China) using a biochar/deionized water suspension mass ratio of 1:20, after stirring for 1.5 h and equilibrating for 1 h. The BET surface area of the biochars was calculated by fitting the N₂ adsorption data to the BET equation. A 0.1000-g aliquot of the biochar sample with a particle size of 200 mesh was outgassed under vacuum (< 0.1 Pa) at 105 °C for 1 h and then heated to 350 °C for 3 h to remove volatiles and moisture. The N₂ adsorption-desorption isotherm was measured under the condition of a liquid nitrogen temperature of -196 °C with a Surface Area and Pore Size Analyzer (NOVA 1200e, Quantachrome, Boynton Beach, USA). A scanning electron microscope (EV018, ZEISS, Oberkochen, Germany) was used to observe the micro-morphologies of the biochars. For the FTIR measurements, 1 mg of slightly ground biochar was gently mixed with 100 mg of oven-dried KBr, and then pressed into a pellet. The FTIR spectra were obtained using a NICOLET 380 FTIR spectrometer (Thermo Electron, Waltham, USA) over the wave number range of 4000 cm⁻¹ to 500 cm⁻¹.

Naphthalene Adsorption Tests

Naphthalene (99%) (J & K Scientific Ltd., Beijing, China) was used to prepare the stock solution by dissolving 0.1 g of naphthalene in 100 mL of 99.5% ethanol. Then, it was diluted to the desired concentration with deionized water containing 10 mmol/L CaCl₂ to simulate environmental water, and 200 mg/L NaN₃ to inhibit biodegradation. The equilibrium concentrations of the naphthalene were determined by an ultraviolet-visible spectrophotometer (UV-2550, SHIMADZU, Kyoto, Japan) at 275 nm.

The effect of the adsorption time on naphthalene removal was studied by adding 2 g/L biochar to 30 mL of a 50 mg/L naphthalene solution in 50.0-mL screw-capped brown bottles. The bottles were placed on a rotating shaker and agitated end-over-end at 30 rpm and 25 °C in the dark for 1 h, 3 h, 6 h, 12 h, 24 h, 48 h, and 72 h to determine at which time equilibrium was reached. Then, the solution was immediately separated from the solids by centrifugation at 4000 rpm for 15 min, and the supernatants were taken to determine the

naphthalene concentration. Because of the negligible adsorption on the glassware and unremarkable losses *via* biodegradation and evaporation, the amount adsorbed by biochar was calculated by the sorbate mass loss from the solution. To investigate the effect of the initial naphthalene concentration, 2 g/L biochar was added to solutions with various naphthalene concentrations (5 mg/L, 10 mg/L, 20 mg/L, 50 mg/L, and 100 mg/L). The samples were shaken at 30 rpm for 72 h before measurement. All of the experiments above were performed in triplicate.

Adsorption Kinetics

To understand the mechanisms of naphthalene adsorption by different biochars, pseudo-first-order (Eqs. 1 and 2) and pseudo-second-order kinetic models (Eqs. 3 and 4) were used to fit the data (Ho and McKay 1998; Ho and McKay 1999),

$$\frac{dq}{dt} = k_1(Q_{e1} - q) \quad (1)$$

$$\log(Q_{e1} - q) = \log Q_{e1} - k_1 t \quad (2)$$

$$\frac{dq}{dt} = k_2(Q_{e2} - q)^2 \quad (3)$$

$$\frac{t}{q} = \frac{1}{k_2 Q_{e2}^2} + \frac{t}{Q_{e2}} \quad (4)$$

where Q_{e1} and Q_{e2} are the amounts of naphthalene adsorbed at equilibrium corresponding to pseudo-first-order and pseudo-second-order adsorption (mg/g), respectively, q denotes the amount of naphthalene adsorbed at time t (mg/g), and k_1 and k_2 are the rate constants for pseudo-first-order and pseudo-second-order adsorption (g/mg·h), respectively.

Adsorption Isotherm

Adsorption isotherms are used to describe how adsorbates interact with adsorbents at equilibrium. The Langmuir and Freundlich isotherm models were used to analyze the experimental data. The Langmuir isotherm model is widely implemented to determine the theoretical value of the maximum adsorption capacity, which assumes monolayer adsorption onto a surface (Langmuir 1918). It can be expressed as,

$$Q_e = \frac{k_L Q_m C_e}{1 + k_L C_e} \quad (5)$$

where Q_e is the amount of naphthalene adsorbed at equilibrium (mg/g), Q_m is the maximum adsorption capacity (mg/g), C_e is the equilibrium concentration of the adsorbate (mg/L), and k_L is the Langmuir constant (L/mg). A dimensionless separation factor (R_L) for the Langmuir isotherm could be calculated with Eq. 6 (Weber and Chakravorti 1974),

$$R_L = 1 / (1 + k_L C_0) \quad (6)$$

where k_L is the Langmuir constant and C_0 is the initial adsorbate concentration (mg/L).

The separation factor indicates if the isotherm is unfavorable ($R > 1$), linear ($R = 1$), favorable ($0 < R < 1$), or irreversible ($R = 0$).

The Freundlich model is an empirical equation that deals with adsorption on

heterogeneous surfaces or surface supporting sites with various affinities. It is assumed that stronger binding sites are occupied first and that the binding strength decreases with an increasing degree of occupation (Freundlich 1907). The Freundlich isotherm equation is,

$$Q_e = k_F C_e^{1/n} \quad (7)$$

where Q_e is the amount of naphthalene adsorbed at equilibrium (mg/g), C_e is the equilibrium concentration of the adsorbate (mg/L), k_F is the Freundlich constant related to the adsorption capacity, and n is the degree of favorability of the adsorption process.

Additionally, $1/n$ ranges between 0 and 1 and is a measure of the adsorption intensity or surface heterogeneity. A lower $1/n$ value indicates a greater degree of heterogeneity on the biochar surface.

Data Analyses

Pearson correlation analyses were conducted to evaluate the relationships between two pyrolytic temperatures, elemental compositions, ash contents, pH values, and BET surface areas, as well as the model parameters of the naphthalene adsorption kinetics and isotherms. The performance of the adsorption kinetic and isotherm models was assessed using the coefficient of determination (R^2), as well as the Akaike information criteria (AIC). When the averaged R^2 is higher and the AIC is lower, the model performs better, and *vice versa*. All of the calculations and plots were performed and generated using MATLAB software (version R2017a, MathWorks, Inc., Natick, USA).

RESULTS AND DISCUSSION

FTIR Spectra and SEM Images of the Biochars

The FTIR spectra of the three types of biochars (W-BC, S-BC, and C-BC) produced at different temperatures are presented in Fig. 1. The peak at 3436 cm^{-1} to 3433 cm^{-1} was assigned to the stretching vibration of the phenolic or alcoholic hydroxyl groups (-OH) (Leng *et al.* 2015); the broad band at 2927 cm^{-1} to 2919 cm^{-1} was assigned to symmetrical and asymmetrical stretching vibrations of aliphatic hydrocarbons or cycloalkanes (-CH₃ and -CH₂) (Leng *et al.* 2015); and the peak at 1650 cm^{-1} to 1580 cm^{-1} was ascribed to C=C and C=O stretching vibration on aromatic rings (Xiao *et al.* 2014). Among these peaks, the sub-strong peak near 1600 cm^{-1} indicated the presence of aromatic C=C or C=O groups in the biochars (Gai *et al.* 2014). The peak near 1630 cm^{-1} is generally considered to be the C=O stretching vibration of alcohol, phenol, and ether (Li *et al.* 2014). Above all, these peaks demonstrated that the surface of the biochar samples may have contained oxygen-containing functional groups, such as carboxyl, carbonyl, and ester groups. The bands at 1440 cm^{-1} and 1380 cm^{-1} corresponded to C=C stretching vibration of lignin and methyl C-H stretching vibration of alkanes, respectively (Wu *et al.* 2012). The peak at 1220 cm^{-1} was designated stretching of aromatic CO- and phenolic -OH. The peak that shifted from 1098 cm^{-1} to 1056 cm^{-1} was assigned to C-O stretching vibration in a carbohydrate or polysaccharide structure, while the peak at 900 cm^{-1} to 750 cm^{-1} was ascribed to C-H bending aromatic CH out-of-plane deformation (Wu *et al.* 2012). In the FTIR spectra of the three different biochars, the same functional groups mentioned above were found around corresponding wavenumbers. Some of the peaks disappeared or shifted. Also, some of them became weak as the pyrolytic temperature increased.

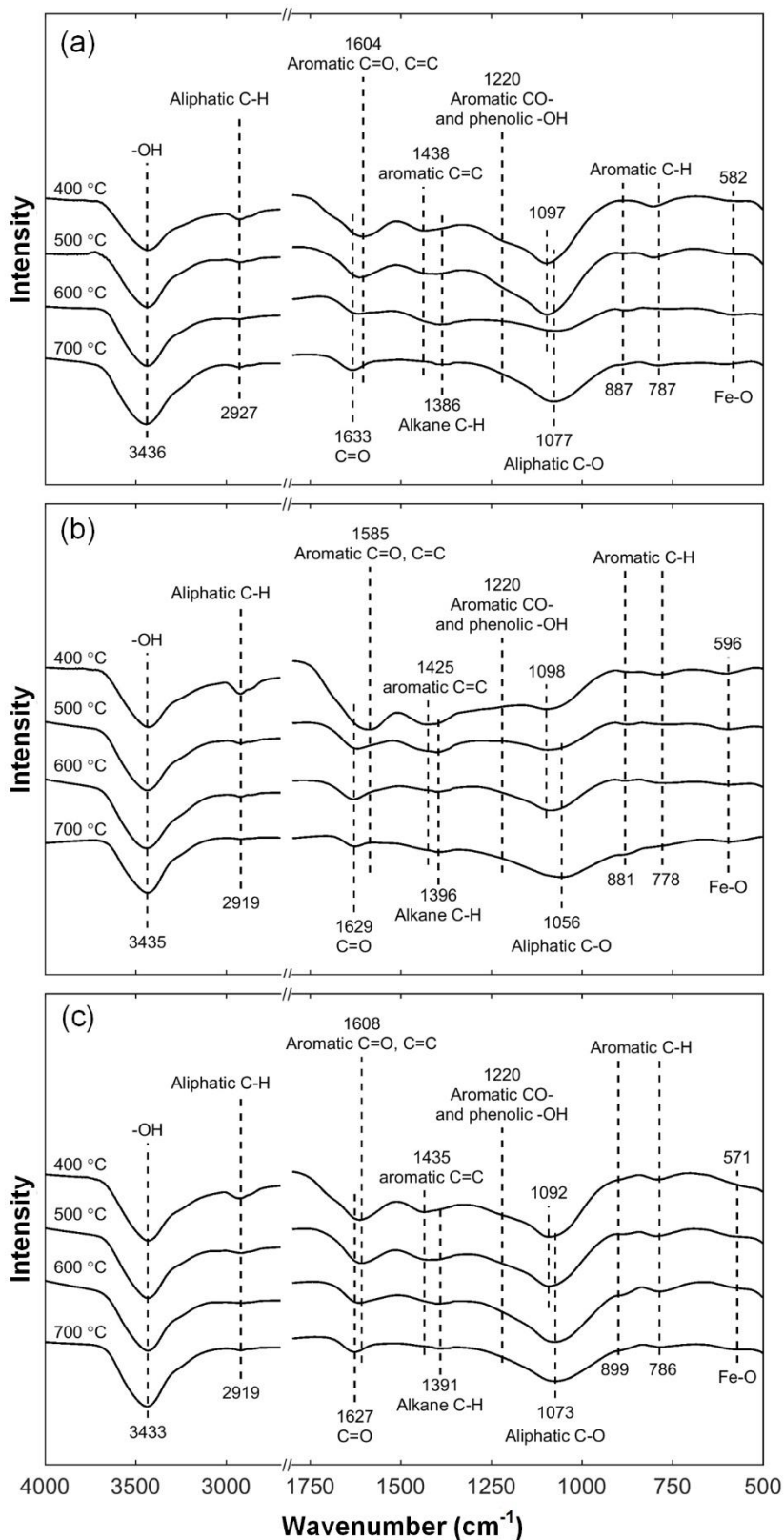


Fig. 1. FTIR spectra of the W-BC (a), S-BC (b), and C-BC (c) prepared from 400 °C to 700 °C

Bands from O-H stretching (3436 cm^{-1} to 3433 cm^{-1}) and aliphatic C-H stretching (2927 cm^{-1} to 2919 cm^{-1}) lost their intensities as the pyrolytic temperature increased from $400\text{ }^{\circ}\text{C}$ to $700\text{ }^{\circ}\text{C}$, which implied accelerated dehydration, greater demethylation (loss of CH_3), and increased decarboxylation (loss of CO_2) in this temperature range (Leng *et al.* 2015). However, a higher pyrolytic temperature resulted in the disappearance of the peak for aromatic CO- and phenolic -OH (approximately 1220 cm^{-1}) and a weaker peak for aromatic C=C (approximately 1440 cm^{-1}) and C-H (900 cm^{-1} to 750 cm^{-1}). This was because of the condensation of the aromatic structure at higher temperatures (Keiluweit *et al.* 2010). Additionally, with a progressively increasing temperature, the straw-derived biochars tended to develop a more stable graphene-like structure, but still maintained a pronounced O-contained functionality. Peaks for aliphatic C-O at 1098 cm^{-1} to 1056 cm^{-1} were detected even at $700\text{ }^{\circ}\text{C}$, which suggested incomplete aromatization and condensation (McBeath and Smernik 2009). The spectra of all three biochars (W-BC, S-BC, and C-BC) were relatively similar, except with slight differences for the peak wavenumbers.

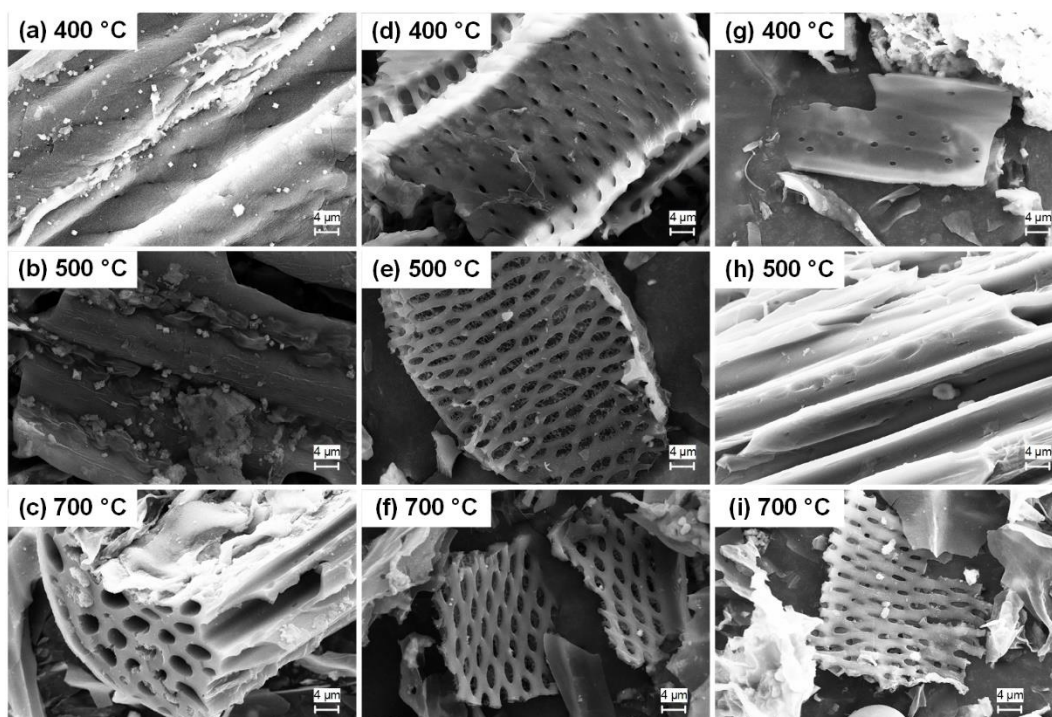


Fig. 2. SEM images of the W-BC (a to c), S-BC (d to f), and C-BC (g to i) produced at $400\text{ }^{\circ}\text{C}$, $500\text{ }^{\circ}\text{C}$, and $700\text{ }^{\circ}\text{C}$ with a residence time of 3 h

The SEM micrographs of the W-BC, S-BC, and C-BC prepared at $400\text{ }^{\circ}\text{C}$, $500\text{ }^{\circ}\text{C}$, and $700\text{ }^{\circ}\text{C}$ with a residence time of 3 h are shown in Fig. 2. The biochars produced from different straw materials had various micro-structures that originally emanated from the plant cells, depending on the intrinsic architecture of the feedstock. Figures 2a to 2c show that the W-BC had a monolithic flaky form when pyrolyzed below $500\text{ }^{\circ}\text{C}$. When the temperature increased from $400\text{ }^{\circ}\text{C}$ to $500\text{ }^{\circ}\text{C}$, the loose and rough surface of the W-BC became smooth with pores. The W-BC prepared at $700\text{ }^{\circ}\text{C}$ had a honey-comb-like structure, which indicated an increased surface area and in turn provided more adsorption sites and space for pollutants. This was because of the easily oxidized organic matter retained in the biochar products produced at low temperatures, which consequently played

a major role in the formation of the microporous structure of biochar at high temperatures (Qian *et al.* 2015). The SEM images of the S-BC revealed a well-developed uniform mesh structure (Figs. 2d to 2f). The pores on the S-BC surface obtained by pyrolysis at 400 °C were relatively small (Fig. 2d). As the temperature increased to 500 °C, the porous structure became more obvious and regular (Fig. 2e). When the temperature increased to 700 °C, the pore structure could be more clearly observed and had less impurities on the surface (Fig. 2f). When the pyrolytic temperature increased from 400 °C to 700 °C, the microscopic structure of the C-BC changed from a monolithic flaky structure to tubular and finally to a reticular form that may have led to an increase in the S_{BET} and active sites (Figs. 2g to 2i).

Table 1. Elemental Compositions, Atomic Ratios, Ash Contents, pH, and Specific Surface Areas of the Biochars Prepared at Different Pyrolytic Temperatures

Biochar	T (°C)	C (%)	H (%)	O (%)	N (%)	O/C	H/C	(N+O)/C	Ash (%)	pH	S_{BET} (m ² /g)
W-BC	400	69.16	5.36	15.08	0.66	0.22	0.08	0.23	9.74	6	4.14
	500	69.44	4.59	13.69	0.52	0.2	0.07	0.2	11.76	9	56.76
	600	71.44	3.3	9.91	0.46	0.14	0.05	0.15	14.89	10	63.21
	700	73.57	2.6	7.65	0.34	0.1	0.04	0.11	15.84	11	72.98
S-BC	400	70.89	5.15	12.19	0.99	0.17	0.07	0.19	10.78	6	5.3
	500	75.78	4.5	5.82	0.74	0.08	0.06	0.09	13.16	10	59.25
	600	77.17	3.19	3.38	0.5	0.04	0.04	0.05	15.76	10	69.47
	700	79.11	2.84	1.39	0.53	0.02	0.04	0.02	16.13	12	83.05
C-BC	400	71.35	5.61	15.17	0.98	0.21	0.08	0.23	6.89	5.5	4.54
	500	73.55	4.89	13.16	0.88	0.18	0.07	0.19	7.52	6	57.95
	600	73.03	3.75	11.14	0.58	0.15	0.05	0.16	11.5	5.5	65.78
	700	75.67	3.06	7.64	0.42	0.1	0.04	0.11	13.21	5.5	101.21

T – Pyrolytic temperature

Elemental Compositions, Ash Contents, pH, and Specific Surface Areas

The elemental compositions, atomic ratios, and S_{BET} values (Table 1) were in line with the FTIR and SEM observations. From 400 °C to 700 °C, the organic carbon content of the biochars increased, while the hydrogen, oxygen, and nitrogen contents decreased. The H/C, O/C, and (N+O)/C atomic ratios decreased because of the progressive dehydration and decarboxylation reactions, which was indicative of the formation of structures containing condensed carbons, such as the aromatic rings inferred from the FTIR spectra (Fig. 1). The biochars prepared at 700 °C were highly carbonized, and highly aromatic structures were formed, as indicated by the low H/C ratios. The lower O/C ratio indicated that the surfaces of the biochars produced at high pyrolytic temperatures were less hydrophilic. The decreased polarity index ((N+O)/C) reflected a decreased polar-group content as the pyrolytic temperature increased (Chen and Chen 2009).

The ash content of the three straw-derived biochars increased remarkably as the temperature increased from 400 °C to 700 °C. Meanwhile, it was noted that the ash contents of the three biochar types were different; they were in the order of: S-BC > W-BC > C-BC. The increase in the ash content resulted from the progressive concentration of minerals (such as K, Na, Ca, Si, and Mg) and destructive volatilization of lignocellulosic matter as the temperature increased (Tsai *et al.* 2012). The higher mineral content in the soybean straw resulted in a higher ash content in the S-BC than in the W-BC and C-BC.

The pH values of all of the biochars produced in this study were between 5.5 and 12. For the different feedstocks, the pH values of the W-BC and C-BC were lower than that of the S-BC. The pH of the W-BC and S-BC increased with a higher pyrolytic temperature, which was consistent with previous findings (Chen *et al.* 2014; Zhang *et al.* 2017). At a low pyrolytic temperature, the pH of the biochars was low because of the production of organic acids and phenolic substances (Yang *et al.* 2018). The increases in the pH with an increasing pyrolytic temperature were attributed to the increase in the ash contents and decrease in organic functional groups, such as -COOH and -OH (Conz *et al.* 2017). For instance, the peak for the stretching vibration of C=O and -OH in carboxyl and phenol became weak or disappeared when the pyrolytic temperature increased from 400 °C to 700 °C. This indicated that the number of acidic groups decreased with an increasing temperature, which explained the increase in the basicity with the pyrolytic temperature for the W-BC and S-BC (Wei *et al.* 2017). However, the peak near 1630 cm^{-1} for the stretching of the aromatic C=O ring may have reflected both acidic and basic groups, whose intensities were still strong at a high temperature. This may have resulted in a relatively stable acidity for the C-BC.

The S_{BET} of the biochar ranged from 1.14 m^2/g to 101.21 m^2/g , which was affected by the feedstock and pyrolytic temperature. When the pyrolytic temperature increased from 400 °C to 500 °C, the S_{BET} values increased remarkably. This was most likely because of the increase in the degree of carbonization, progressive destruction of aliphatic alkyl and ester groups, and formation of micropores in the biochar, which could have hidden the aromatic core at higher temperatures (Chen *et al.* 2008). The reticular S-BC provided more surface area than the tubular C-BC and flaky W-BC produced at a moderate pyrolytic temperature (500 °C), and the C-BC was more porous than the S-BC and W-BC produced at a higher pyrolytic temperature (700 °C), which was inconsistent with the SEM observations.

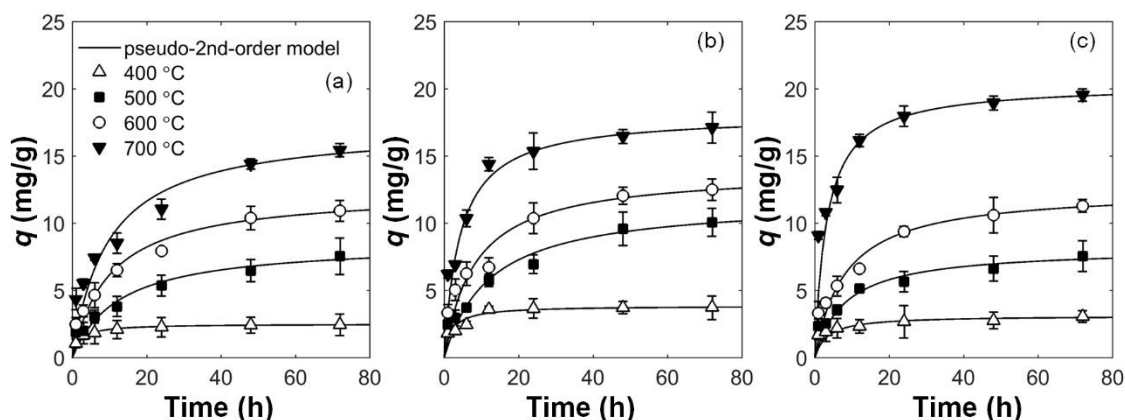


Fig. 3. Pseudo-second-order kinetics for naphthalene adsorption by the W-BC (a), S-BC (b), and C-BC (c) prepared at 400 °C to 700 °C with a residence time of 3 h

Adsorption Kinetics and Isotherms

The naphthalene adsorption process was time-dependent for all of the tested biochars (Fig. 3). It was found that the adsorption of naphthalene was fast within the first 12 h of adsorbent–adsorbate contact. Then, the adsorption rate decreased gradually until it almost reached an equilibrium around 48 h and became stable after 72 h. A great number of unoccupied adsorption sites and the high adsorbate concentration gradient at the

beginning of the adsorption process promoted the rapid initial uptake (Yang *et al.* 2018). With the extension of the contact time, adsorption approached equilibrium. The maximum adsorption capacities were in line with the S_{BET} values of the biochars in the present study.

Table 2. Kinetic Parameters for Naphthalene Adsorption by the Biochars Produced at Different Pyrolytic Temperatures

Biochar	T (°C)	Pseudo-first-order Model				Pseudo-second-order Model			
		Q_{e1} (mg/g)	k_1 (g/mg·h)	R^2	AIC	Q_{e2} (mg/g)	k_2 (g/mg·h)	R^2	AIC
W-BC	400	2.273	0.481	0.85	-0.29	2.529	0.207	0.99	-7.47
	500	6.94	0.08	0.89	18.74	8.591	0.009	0.97	15.76
	600	10.3	0.093	0.91	22.5	12.4	0.008	0.98	18
	700	14.07	0.107	0.81	31.46	17.23	0.006	0.95	28.22
S-BC	400	3.654	0.291	0.75	11.23	3.878	0.134	0.86	7.4
	500	9.638	0.078	0.9	22.5	11.73	0.007	0.97	19.48
	600	11.79	0.112	0.84	27.97	13.93	0.009	0.95	24.61
	700	16.22	0.199	0.89	28.46	18.1	0.013	0.96	25.77
C-BC	400	2.584	0.823	0.47	8.17	3.142	0.097	0.9	11.93
	500	6.704	0.139	0.84	19.77	8.163	0.015	0.96	17.37
	600	10.6	0.113	0.87	25.07	12.51	0.01	0.96	21.72
	700	17.94	0.318	0.7	34.32	20.36	0.015	0.95	31.15

Residence time = 3 h; initial naphthalene concentration = 50 mg/L; and biochar application rate = 2 g/L

Pseudo-first-order and pseudo-second-order models were applied to study the kinetics of the adsorption process. Table 2 shows that the naphthalene adsorption kinetics of all three types of biochars prepared at different temperatures. The pseudo-second-order model resulted in a better fit for the experimental data with a higher R^2 and smaller AIC. The calculated adsorption capacities of all of the tested biochars closely matched their corresponding experimental measurements.

The sorbent structural characteristics (*e.g.*, aromaticity and polarity) and sorbate properties (*i.e.*, molecule size and octanol-water partition coefficient) had an important effect on the adsorption kinetic behavior (Xi and Chen 2014). Generally, the S-BC showed a greater adsorption capacity (Q_{e2}) and faster adsorption rate (k_2) compared with the W-BC and C-BC. The adsorption rates (k_2) of the naphthalene for the biochars prepared at 400 °C were relatively faster than those produced at higher temperatures. This meant the adsorption processes of the biochars prepared at 400 °C reached equilibrium more quickly than the others. However, the amounts of naphthalene adsorbed at equilibrium (Q_{e1} and Q_{e2}) were relatively lower for the biochars pyrolyzed at a lower temperature.

The naphthalene adsorption isotherm data was fitted to the Freundlich and Langmuir models. The increase in the initial naphthalene concentration acted as the driving force for naphthalene to overcome the transfer resistances between the solution and biochars, and provide a high contact probability between the biochar and naphthalene, which resulted in an increase in the adsorption capacity. As the limited active sites (micropores and π -electron densities) on the biochars became saturated at a relatively higher concentration, the increase in the adsorption capacity was restricted (Fig. 4) (Ania *et al.* 2007).

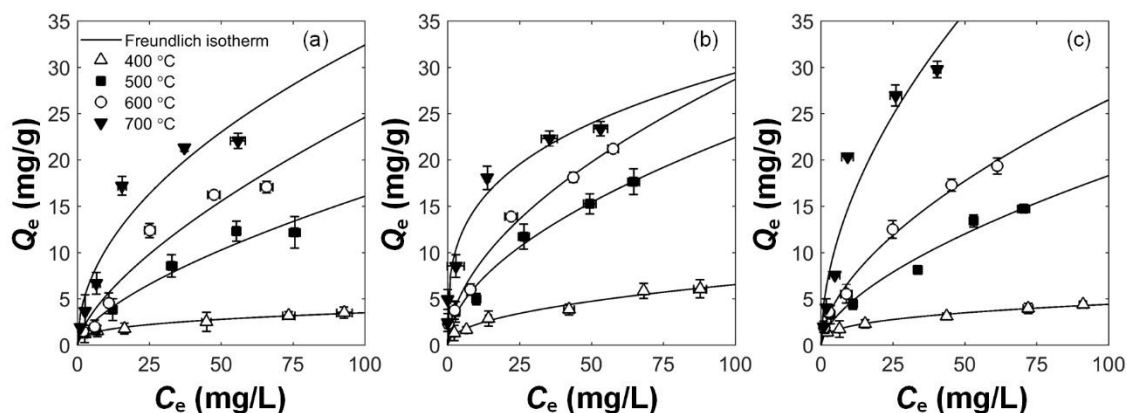


Fig. 4. Freundlich isotherms for naphthalene adsorption by the W-BC (a), S-BC (b), and C-BC (c) prepared at 400 °C to 700 °C with a residence time of 3 h

Table 3. Isotherm Parameters for Naphthalene Adsorption by the Biochars Produced at Different Pyrolytic Temperatures

Biochar	T (°C)	Langmuir Parameters					Freundlich Parameters			
		Q_m (mg/g)	k_L (L/mg)	R^2	AIC	R_L range	k_F $\text{mg}^{(1-1/n)}$ $\text{L}^{1/n}/\text{g}$	$1/n$	R^2	AIC
W-BC	400	3.558	0.098	0.85	8	0.09 - 0.67	0.789	0.325	0.98	-3.67
	500	22	0.019	0.98	15.65	0.34 - 0.91	0.822	0.646	0.96	20.02
	600	30.98	0.021	0.97	22.56	0.32 - 0.90	1.168	0.662	0.94	26.43
	700	29.59	0.064	0.97	25.35	0.14 - 0.76	3.328	0.494	0.92	31.51
S-BC	400	7.535	0.041	0.93	12.47	0.20 - 0.83	0.772	0.465	0.97	6.61
	500	26.79	0.028	0.96	22.48	0.26 - 0.88	1.861	0.541	0.98	18.71
	600	30.77	0.036	0.98	22.01	0.22 - 0.85	2.404	0.539	0.99	18.86
	700	25.66	0.183	0.94	29.69	0.05 - 0.52	7.566	0.295	0.98	23.76
C-BC	400	4.493	0.093	0.88	9.72	0.10 - 0.68	0.947	0.335	0.99	-3.77
	500	27.46	0.016	0.95	22.6	0.38 - 0.93	1.115	0.608	0.97	18.31
	600	29.96	0.03	0.99	16.93	0.25 - 0.87	1.832	0.58	0.99	14.62
	700	40.59	0.075	0.97	29.79	0.12 - 0.73	4.469	0.533	0.92	34.71

Residence time = 3 h; biochar application rate = 2 g/L; and contact time = 72 h

The parameters of each isotherm model are given in Table 3. Both the Freundlich and Langmuir isotherm models confirmed that naphthalene adsorption by all three biochars were effective. The dimensionless separation factor R_L derived from the Langmuir isotherm was between 0 and 1 for each biochar, which suggested that adsorption was favorable. Normally, the extent of biochar carbonization caused by the pyrolytic temperature has a strong impact on the adsorption mechanism because adsorption to the various subdomains of biochar can occur by different linear and nonlinear mechanisms (Chen *et al.* 2008). The Freundlich model had higher R^2 values for the S-BC (400 °C to 700 °C) and C-BC (400 °C to 600 °C), but the Langmuir model fit better for the W-BC (500 °C to 700 °C) and C-BC (700 °C). This may have suggested that the adsorption of naphthalene to the S-BC and C-BC was generally not dependent on monolayer adsorption

temperature and S_{BET} . It significantly correlated with the aromaticity, hydrophilicity, and polarity of the biochars.

For the adsorption isotherms, all three biochars exhibited a significant change in the adsorption capacity (Q_{m} and k_{F}) for naphthalene after the pyrolytic temperature increased, which was in line with the surface and elemental characteristics (Table 1). The Langmuir adsorption capacity (Q_{m}) also showed a significant correlation with the biochar S_{BET} values, elemental composition, and ash content. It positively correlated with the kinetic adsorption capacities (Q_{e1} and Q_{e2}), but negatively correlated with the adsorption rates (k_1 and k_2). The Freundlich constant (k_{F}) also significantly correlated with the ash content and elemental compositions, except for the N content. It showed an exponential relationship with the biochar S_{BET} ($k_{\text{F}} = 9.68 \times 10^{-4} \times \exp(0.107 \times S_{\text{BET}}) + 0.773$, $R^2 = 0.98$), and positively correlated with Q_{e1} and Q_{e2} . Negative correlations for the $\log(k_{\text{F}})$ values with the aromaticity ($y = -17.34x + 1.20$, $R^2 = 0.75$) and polarity index ($y = -4.15x + 0.82$, $R^2 = 0.75$) were observed for all of the biochars.

Naphthalene adsorption on biochar is generally dependent on capacity (number of active sites) and affinity (bonding strength). It is well known that the micropores of the adsorbents, particularly those of narrower diameter, are active sites for the retention of naphthalene (Ania *et al.* 2007). The increased S_{BET} increased the quantity of active sites on the biochar surface (Table 1), which could be proved by the significantly positive correlation between S_{BET} and adsorption capacity (Q_{m} and k_{F}) (Fig. 5). Furthermore, naphthalene molecules may interact specifically with the carbon surface due to their polyaromatic structure, involving interactions of the electron-rich regions located in the graphene layers with the π -electrons of the adsorbate (Ania *et al.* 2007). The higher π -electron densities arising from the low oxygen contents result in a larger adsorption of naphthalene from liquid phase (Table 1) (Ania *et al.* 2007). However, the contribution of such π -electron active sites for S-BC is probably less than that for other two biochars, as indicating by their regression slopes (-1.96, -3.13 and -4.32 for S-BC, W-BC and C-BC, respectively) between Q_{m} and oxygen content.

In contrast to adsorption capacity, the k_{L} , which was representative of the bonding strength between the naphthalene molecules and biochar surface, showed no significant correlation with any of the other parameters. The k_{L} value decreased first, and then it increased with an increase in the pyrolytic temperature. This indicated that the combinations of the naphthalene molecules and biochar surface were relatively weak at a moderate pyrolytic temperature (500 °C). For the biochars pyrolyzed at a low temperature (400 °C), the S_{BET} was low, which indicated a small porosity, but the atomic ratio of (N+O)/C was relatively high and contributed to the high polarity. Even though naphthalene is a nonpolar molecule, its accessibility to polar surface pores would be interfered with by adsorbed water, which may have accounted for the high bonding strength between the naphthalene molecules and biochar surface (Chun *et al.* 2004). With an increase in the pyrolytic temperature, the S_{BET} increased rapidly and the surface polarity-controlled combination progressively changed to a porosity-controlled combination. Note that the relatively higher k_{L} values of S-BC implied stronger naphthalene adsorption affinity, and might also explain its greater adsorption capacity (Q_{e2}) and faster adsorption rate (k_2) compared with that of W-BC and C-BC.

The heterogeneity factor $1/n$ of the Freundlich model increased first, and then decreased with an increase in the pyrolytic temperature, which indicated less heterogeneity on the biochar surface prepared at moderate temperatures (500 °C to 600 °C). It did not significantly correlate with the pyrolytic temperature and biochar properties, and

negatively correlated with the adsorption rates and k_L . It should be noted that the $1/n$ value ranged between 0 and 1, which led to favorable adsorption (Kong *et al.* 2014).

CONCLUSIONS

1. The results of this study indicated that the pyrolytic temperature and feedstock type greatly influenced the chemical and physical characteristics of the biochar, which in turn influenced its naphthalene adsorption ability.
2. Among all biochars prepared at moderate temperatures, the S-BC generally had a higher ash content, greater pH value, and provided more surface area. This resulted in a higher carbonization degree, weaker aromaticity, hydrophilicity, and polarity, and consequently a greater naphthalene adsorption capacity and faster adsorption rate than for the W-BC and C-BC.
3. The analyses on adsorption kinetics and isotherms, as well as correlations between the adsorption capability, affinity and rates, and the characteristics of the biochars provided theoretical bases for revealing the adsorption mechanisms, and would be helpful in selecting crop residues and optimizing pyrolytic temperatures with a high naphthalene removal efficiency.

ACKNOWLEDGMENTS

The authors are grateful for the support of the Fundamental Research Funds for the Central Universities (Grant No. N172504021), the Science and Technology Planning Project of Guangdong Province (Grant No. 2017B030314092), and the National Key Research and Development Program (Grant No. 2018YFC1801200).

REFERENCES CITED

- Ahmad, M., Rajapaksha, A. U., Lim, J. E., Zhang, M., Bolan, N., Mohan, D., Vithanage, M., Lee, S. S., and Ok, Y. S. (2014). "Biochar as a sorbent for contaminant management in soil and water: A review," *Chemosphere* 99, 19-33. DOI: 10.1016/j.chemosphere.2013.10.071
- Ali, O. A., and Tarek, S. J. (2012). "Removal of polycyclic aromatic hydrocarbons from Ismailia Canal water by chlorine, chlorine dioxide and ozone," *Desalin. Water Treat.* 1(1-3), 289-298. DOI: 10.5004/dwt.2009.131
- Ania, C. O., Cabal, B., Pevida, C., Arenillas, A., Parra, J. B., Rubiera, F., and Pis, J. J. (2007). "Removal of naphthalene from aqueous solution on chemically modified activated carbons," *Water Res.* 41(2), 333-40. DOI: 10.1016/j.watres.2006.10.016
- ASTM. (2007). D 1762-84: "Standard method for chemical analysis of wood charcoal," American Society for Testing and Materials International. West Conshohocken, PA, USA.
- Bayazit, Ş. S., Yildiz, M., Aşçi, Y. S., Şahin, M., Bener, M., Eğlence, S., and Abdel Salam, M. (2017). "Rapid adsorptive removal of naphthalene from water using

- graphene nanoplatelet/MIL-101 (Cr) nanocomposite," *J. Alloy. Compd.* 701, 740-749. DOI: 10.1016/j.jallcom.2017.01.111
- Cha, J. S., Park, S. H., Jung, S. C., Ryu, C., Jeon, J.-K., Shin, M. C., and Park, Y. K. (2016). "Production and utilization of biochar: A review," *J. Ind. Eng. Chem.* 40, 1-15. DOI: 10.1016/j.jiec.2016.06.002
- Changchaivong, S., and Khaodhiar, S. (2009). "Adsorption of naphthalene and phenanthrene on dodecylpyridinium-modified bentonite," *Appl. Clay Sci.* 43(3-4), 317-321. DOI: 10.1016/j.clay.2008.09.012
- Chen, B., and Chen, Z. (2009). "Sorption of naphthalene and 1-naphthol by biochars of orange peels with different pyrolytic temperatures," *Chemosphere* 76(1), 127-133. DOI: 10.1016/j.chemosphere.2009.02.004
- Chen, Z., Chen, B., and Chiou, C. T. (2012). "Fast and slow rates of naphthalene sorption to biochars produced at different temperatures," *Environ. Sci. Technol.* 46(20), 11104-11. DOI: 10.1021/es302345e
- Chen, B., Zhou, D., and Zhu, L. (2008). "Transitional adsorption and partition of nonpolar and polar aromatic contaminants by biochars of pine needles with different pyrolytic temperatures," *Environ. Sci. Technol.* 42(14), 5137-5143. DOI: 10.1021/es8002684
- Chen, J., Li, C., Ristovski, Z., Milic, A., Gu, Y., Islam, M. S., Wang, S., Hao, J., Zhang, H., He, C., *et al.* (2017). "A review of biomass burning: Emissions and impacts on air quality, health and climate in China," *Sci. Total Environ.* 579, 1000-1034. DOI: 10.1016/j.scitotenv.2016.11.025
- Chen, T., Zhang, Y., Wang, H., Lu, W., Zhou, Z., Zhang, Y., and Ren, L. (2014). "Influence of pyrolysis temperature on characteristics and heavy metal adsorptive performance of biochar derived from municipal sewage sludge," *Bioresour. Technol.* 164, 47-54. DOI: 10.1016/j.biortech.2014.04.048
- Chun, Y., Sheng, G., Chiou, C. T., and Xing, B. (2004). "Compositions and sorptive properties of crop residue-derived chars," *Environ. Sci. Technol.* 38(17), 4649-4655. DOI: 10.1021/es035034w
- Conz, R. F., Abbruzzini, T. F., de Andrade, C. A., Milori, D. M. B. P., and Cerri, C. E. P. (2017). "Effect of pyrolysis temperature and feedstock type on agricultural properties and stability of biochars," *Agricultural Sciences* 8(9), 914-933. DOI: 10.4236/as.2017.89067
- Cooper, W. J., Nickelsen, M. G., Green, R. V., and Mezyk, S. P. (2002). "The removal of naphthalene from aqueous solutions using high-energy electron beam irradiation". *Radiat. Phys. Chem.* 65(4-5), 571-577. DOI: 10.1016/S0969-806X(02)00363-8
- Freundlich, H. (1907). "Über die Adsorption in Lösungen [About adsorption in solutions]," *Zeitschrift für Physikalische Chemie* 57U(1), 385-490. DOI: 10.1515/zpch-1907-5723
- Gai, X., Wang, H., Liu, J., Zhai, L., Liu, S., Ren, T., and Liu, H. (2014). "Effects of feedstock and pyrolysis temperature on biochar adsorption of ammonium and nitrate," *PLoS ONE* 9(12). DOI: 10.1371/journal.pone.0113888
- Goel, R. K., Flora, J. R. V., and Ferry, J. (2003). "Mechanisms for naphthalene removal during electrolytic aeration," *Water Res.* 37(4), 891-901. DOI: 10.1016/S0043-1354(02)00376-7

- Han, L., Ro, K. S., Wang, Y., Sun, K., Sun, H., Libra, J. A., and Xing, B. (2018). "Oxidation resistance of biochars as a function of feedstock and pyrolysis condition," *Sci. Total Environ.* 616-617, 335-344. DOI: 10.1016/j.scitotenv.2017.11.014
- Ho, Y. S., and McKay, G. (1998). "Sorption of dye from aqueous solution by peat," *Chem. Eng. J.* 70(2), 115-124. DOI: 10.1016/S0923-0467(98)00076-1
- Ho, Y. S., and McKay, G. (1999). "Pseudo-second order model for sorption processes," *Process Biochem.* 34(5), 451-465. DOI: 10.1016/S0032-9592(98)00112-5
- Keiluweit, M., Nico, P. S., Johnson, M. G., and Kleber, M. (2010). "Dynamic molecular structure of plant biomass-derived black carbon (biochar)," *Environ. Sci. Technol.* 44(4), 1247-1253. DOI: 10.1021/es9031419
- Kong, J., Yue, Q., Sun, S., Gao, B., Kan, Y., Li, Q., and Wang, Y. (2014). "Adsorption of Pb(II) from aqueous solution using keratin waste – hide waste: Equilibrium, kinetic and thermodynamic modeling studies," *Chem. Eng. J.* 241, 393-400. DOI: 10.1016/j.cej.2013.10.070
- Langmuir, I. (1918). "The adsorption of gases on plane surfaces of glass, mica and platinum," *J. Am. Chem. Soc.* 40(9), 1361-1403. DOI: 10.1021/ja02242a004
- Leng, L., Yuan, X., Huang, H., Shao, J., Wang, H., Chen, X., and Zeng, G. (2015). "Biochar derived from sewage sludge by liquefaction: Characterization and application for dye adsorption," *Appl. Surf. Sci.* 346, 223-231. DOI: 10.1016/j.apsusc.2015.04.014
- Li, H., Mahyoub, S. A. A., Liao, W., Xia, S., Zhao, H., Guo, M., and Ma, P. (2017). "Effect of pyrolysis temperature on characteristics and aromatic contaminants adsorption behavior of magnetic biochar derived from pyrolysis oil distillation residue," *Bioresour. Technol.* 223, 20-26. DOI: 10.1016/j.biortech.2016.10.033
- Li, H., Qu, R., Li, C., Guo, W., Han, X., He, F., Ma, Y., and Xing, B. (2014). "Selective removal of polycyclic aromatic hydrocarbons (PAHs) from soil washing effluents using biochars produced at different pyrolytic temperatures," *Bioresour. Technol.* 163, 193-198. DOI: 10.1016/j.biortech.2014.04.042
- Mandal, S., Donner, E., Vasileiadis, S., Skinner, W., Smith, E., and Lombi, E. (2018). "The effect of biochar feedstock, pyrolysis temperature, and application rate on the reduction of ammonia volatilisation from biochar-amended soil," *Sci. Total Environ.* 627, 942-950. DOI: 10.1016/j.scitotenv.2018.01.312
- McBeath, A. V., and Smernik, R. J. (2009). "Variation in the degree of aromatic condensation of chars," *Org. Geochem.* 40(12), 1161-1168. DOI: 10.1016/j.orggeochem.2009.09.006
- Mehmood, K., Chang, S., Yu, S., Wang, L., Li, P., Li, Z., Liu, W., Rosenfeld, D., and Seinfeld, J. H. (2018). "Spatial and temporal distributions of air pollutant emissions from open crop straw and biomass burnings in China from 2002 to 2016," *Environ. Chem. Lett.* 16(1), 301-309. DOI: 10.1007/s10311-017-0675-6
- Pan, J., Jiang, J., and Xu, R. (2013). "Adsorption of Cr(III) from acidic solutions by crop straw derived biochars," *J. Environ. Sci.-China* 25(10), 1957-1965. DOI: 10.1016/s1001-0742(12)60305-2
- Qian, L., Chen, M., and Chen, B. (2015). "Competitive adsorption of cadmium and aluminum onto fresh and oxidized biochars during aging processes," *J. Soils Sediments* 15(5), 1130-1138. DOI: 10.1007/s11368-015-1073-y
- Rodríguez-Vila, A., Selwyn-Smith, H., Enunwa, L., Smail, I., Covelo, E. F., and Sizmur, T. (2018). "Predicting Cu and Zn sorption capacity of biochar from feedstock C/N ratio and pyrolysis temperature," *Environ. Sci. Pollut. R.* 25(8), 7730-7739. DOI: 10.1007/s11356-017-1047-2

- Tran, H. N., You, S. J., and Chao, H. P. (2016). "Effect of pyrolysis temperatures and times on the adsorption of cadmium onto orange peel derived biochar," *Waste Manage. Res.* 34(2), 129-138. DOI: 10.1177/0734242X15615698
- Tsai, W. T., Liu, S. C., Chen, H. R., Chang, Y. M., and Tsai, Y. L. (2012). "Textural and chemical properties of swine-manure-derived biochar pertinent to its potential use as a soil amendment," *Chemosphere* 89(2), 198-203. DOI: 10.1016/j.chemosphere.2012.05.085
- Wang, M., Zhu, Y., Cheng, L., Anderson, B., Zhao, X., Wang, D., and Ding, A. (2018). "Review on utilization of biochar for metal-contaminated soil and sediment remediation," *J. Environ. Sci.-China* 63, 156-173. DOI: 10.1016/j.jes.2017.08.004
- Weber, T. W., and Chakravorti, R. K. (1974). "Pore and solid diffusion models for fixed-bed adsorbers," *AIChE J.* 20(2), 228-238. DOI: 10.1002/aic.690200204
- Wei, S., Zhu, M., Song, J., and Peng, P. (2017). "Comprehensive characterization of biochars produced from three major crop straws of China," *BioResources* 12(2), 3316-3330. DOI: 10.15376/biores.12.2.3316-3330
- Wu, W., Yang, M., Feng, Q., McGrouther, K., Wang, H., Lu, H., and Chen, Y. (2012). "Chemical characterization of rice straw-derived biochar for soil amendment," *Biomass Bioenerg.* 47, 268-276. DOI: 10.1016/j.biombioe.2012.09.034
- Xi, Z., and Chen, B. (2014). "Removal of polycyclic aromatic hydrocarbons from aqueous solution by raw and modified plant residue materials as biosorbents," *J. Environ. Sci.-China* 26(4), 737-748. DOI: 10.1016/s1001-0742(13)60501-x
- Xiao, L., Bi, E., Du, B., Zhao, X., and Xing, C. (2014). "Surface characterization of maize-straw-derived biochars and their sorption performance for MTBE and benzene," *Environ. Earth Sci.* 71(12), 5195-5205. DOI: 10.1007/s12665-013-2922-x
- Yang, H. I., Lou, K., Rajapaksha, A. U., Ok, Y. S., Anyia, A. O., and Chang, S. X. (2018). "Adsorption of ammonium in aqueous solutions by pine sawdust and wheat straw biochars," *Environ. Sci. Pollut. R.* 25(26), 25638-25647. DOI: 10.1007/s11356-017-8551-2
- Yang, W., Wang, Y., Sharma, P., Li, B., Liu, K., Liu, J., Flury, M., and Shang, J. (2017). "Effect of naphthalene on transport and retention of biochar colloids through saturated porous media," *Colloid. Surface. A.* 530, 146-154. DOI: 10.1016/j.colsurfa.2017.07.010
- Yuan, J. H., Xu, R. K., and Zhang, H. (2011). "The forms of alkalis in the biochar produced from crop residues at different temperatures," *Bioresour. Technol.* 102(3), 3488-3497. DOI: 10.1016/j.biortech.2010.11.018
- Zhang, G., Zhang, Q., Sun, K., Liu, X., Zheng, W., and Zhao, Y. (2011). "Sorption of simazine to corn straw biochars prepared at different pyrolytic temperatures," *Environ. Pollut.* 159(10), 2594-2601. DOI: 10.1016/j.envpol.2011.06.012
- Zhang, H., Chen, C., Gray, E. M., and Boyd, S. E. (2017). "Effect of feedstock and pyrolysis temperature on properties of biochar governing end use efficacy," *Biomass Bioenerg.* 105, 136-146. DOI: 10.1016/j.biombioe.2017.06.024
- Zhang, J., Liu, J., and Liu, R. (2015). "Effects of pyrolysis temperature and heating time on biochar obtained from the pyrolysis of straw and lignosulfonate," *Bioresour. Technol.* 176, 288-291. DOI: 10.1016/j.biortech.2014.11.011

Zhang, Y. L., and Cao, F. (2015). “Is it time to tackle PM_{2.5} air pollutions in China from biomass-burning emissions?,” *Environ. Pollut.* 202, 217-219. DOI: 10.1016/j.envpol.2015.02.005

Article submitted: December 11, 2018; Peer review completed: February 10, 2019;
Revised version received and accepted: February 16, 2019; Published: February 20, 2019.
DOI: 10.15376/biores.14.2.2885-2902